Magnetostatic spin wave modes in trilayer nanowire arrays probed using ferromagnetic resonance spectroscopy

X. Zhou and A. O. Adeyeye*

Information Storage Materials Laboratory, Department of Electrical and Computer Engineering, National University of Singapore, Singapore 117576

(Received 26 April 2016; revised manuscript received 9 June 2016; published 9 August 2016)

We investigate the spin wave modes in asymmetric trilayer [$Ni_{80}Fe_{20}$ (10 nm)/Cu(t_{Cu})/$Ni_{80}Fe_{20}$ (30 nm)] nanowire structures as a function of the Cu thickness (t_{Cu}) in the range from 0 to 20 nm using perpendicular ferromagnetic resonance (pFMR) spectroscopy. For $t_{Cu} = 0$ nm, corresponding to the 40 nm thick single layer $Ni_{80}Fe_{20}$ nanowires, both the fundamental and first order modes are observed in the saturation region. However, for the trilayer structures, two additional modes, which are the fundamental and first order optical modes, are observed. We also found that the resonance fields of these modes are markedly sensitive to the Cu thickness due to the competing effects of interlayer exchange coupling and magnetostatic dipolar coupling. When the $t_{Cu} \geqslant 10$ nm, the fundamental optical mode is more pronounced. Our experimental results are in quantitative agreement with the dynamic micromagnetic simulations.

DOI: 10.1103/PhysRevB.94.054410

I. INTRODUCTION

In the last few decades, the subject of spin waves in patterned nanostructures has been extensively studied both from a fundamental viewpoint [1–4] and because of their potential use in applications such as magnetic memory units [5], microwave filters [6], and other low power consumption spintronic devices [7–9]. Ferromagnetic (FM) nanowires have especially attracted intensive attention due to its strong shape anisotropy [10–12], potential use for manipulation of spin wave propagation [13,14], and magnonics [10,15,16]. There have also been reports on the theory of collective spin wave excitation in interacting homogeneous nanowire arrays [2,17] and alternating width nanowires [18], observation of frequency band gap in both homogenous nanowires [19–21], and synthetic nanostructured crystals with NiFe and Co nanowires in contact laterally [22–24]. These studies have shown that the magnetic properties of nanowires could be significantly modified by tuning the width of the nanowire, interwire gap, and the magnetic materials.

The effects of interlayer exchange coupling and magnetostatic coupling on the dynamic behavior of multilayer nanowires have also been studied [25–29]. The coupling mechanism within multilayer structures plays an important role in determining the magnetization ground states and the dynamic responses [30,31]. The oscillating interlayer exchange coupling, showing either FM or antiferromagnetic (AFM) coupling with varied nonmagnetic spacer layer thickness, can be used to obtain either FM or AFM ground states [26]. Recently, it has also been reported [27,28] that in a multilayer system with magnetostatic coupling only, the magnetization groud states can also be significantly modified by tuning the thickness of the magnetic layer. However, so far there has been no systematic study on how the competition between dipolar coupling and interlayer exchange coupling affects the dynamic response in trilayer nanowires. Moreover, to the best of our knowledge, most of the works have been focused on studying the magnetic properties of multilayer nanowires with the external magnetic field applied in plane. Only very limited research work [32] has been reported on the dynamic behaviors of trilayer nanowire arrays with the magnetic bias field applied out of plane, whereby the high in-plane symmetry is preserved [33].

Ferromagnetic resonance (FMR) spectroscopy is a powerful technique to explore the dynamic behavior of FM nanostructures [32,34,35] and determine the magnetic properties [36–38], such as effective demagnetizing factors, interlayer coupling strength, and so on. In this paper, we performed a systematical investigation on the dynamic properties of asymmetric trilayer nanowire structures $Ni_{80}Fe_{20}$ (10 nm)/Cu(t_{Cu})/$Ni_{80}Fe_{20}$ (30 nm) with Cu thickness varied in the range from 0 to 20 nm using perpendicular FMR (pFMR). Different from the conventional vector network analyzer (VNA)-FMR, pFMR is a high sensitivity characterization technique [39,40] for which a phase bridge is used to eliminate the background fluctuation coming from the microwave source. The utilization of the ac modulation technique also ensures that the system is immune to the nonmagnetic background signal. These capabilities help to resolve the resonance signal better and thus enable us to detect weak modes resulting from inhomogeneous magnetization.

We observed both the fundamental and first order modes in the saturation region for the 40 nm thick single layer $Ni_{80}Fe_{20}$ nanowires (corresponding to $t_{Cu} = 0$). For the trilayer structures, we found two additional modes, which are the fundamental and first order optical modes. These modes are very sensitive to the Cu thickness. We observed good quantitative agreement between our experimental results and dynamic micromagnetic simulations.

II. EXPERIMENTAL AND SIMULATION DETAILS

Large area (4×4 mm^2) periodic arrays of asymmetric trilayer [$Ni_{80}Fe_{20}$ (10 nm)/Cu(t_{Cu})/$Ni_{80}Fe_{20}$ (30 nm] nanowires with varied spacer layer thickness were fabricated on a silicon substrate using deep ultraviolet lithography (DUV) at 193 nm

*Corresponding author: eleaao@nus.edu.sg

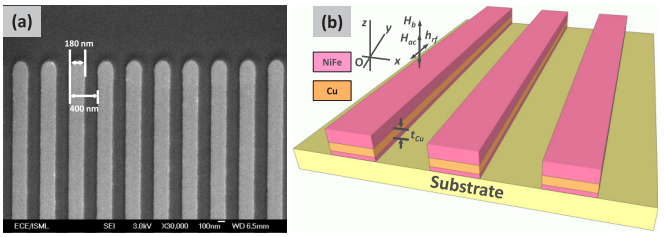

FIG. 1. (a) The SEM image of nanowire arrays. The nanowire width is $w = 180$ nm, pitch is $p = 400$ nm. (b) A sketch of the trilayer nanowire structures $Ni_{80}Fe_{20}$ (10 nm)/Cu(t_{Cu})/$Ni_{80}Fe_{20}$ (30 nm).

exposure wavelength followed by electron beam evaporation and ultrasonic assisted lift off process in OK73 resist thinner. The materials were deposited at a constant rate of 0.2 Å s^{-1} in a chamber with a base pressure of 4×10^{-8} Torr. Details of the lithographic process developed for the DUV lithography at 248 nm exposure wavelength adapted for this work has been described elsewhere [41]. Scanning electron microscope (SEM) was used to verify the successful lift off and the actual dimensions of the nanowire arrays. The representative SEM image for nanowires fabricated from the same template is shown in Fig. 1(a). The width of the nanowire is 180 nm, and the pitch is 400 nm. A schematic of the trilayer structure is shown in Fig. 1(b).

The dynamic response was characterized using pFMR at room temperature. A 20 dBm microwave signal was generated by a continuous wave (c.w.) microwave generator at a specific frequency in the range from 6 GHz to 16 GHz. The samples were placed on top of a 50 Ω microstrip line with the nanowire arrays facing the stripeline. The magnetic bias field (H_b) was swept from 18 kOe to 0 with an ac modulating field of ±20 Oe(H_{ac}) applied perpendicularly to the film plane (defined as z direction). A sketch of the field geometry is shown as the inset of Fig. 1(b). The output dc signal of the interferometric device is fed into a digital lock-in amplifier locked to the field modulation signal. The FMR signal detected in this way represents the first derivative of the field sweeping absorption curve at a selected frequency.

To validate the experimental results, we performed dynamic micromagnetic simulation using the LLG micomagnetic simulator [42]. Standard parameters for $Ni_{80}Fe_{20}$ (Landau-Lifshitz gyromagnetic ratio $|\gamma|$ of 2.8 GHz kOe^{-1}, exchange constant A of 1.30×10^{-6} erg · cm^{-1}, damping constant α of 0.01, anisotropy constant $K_U = 0$, and saturation magnetization Ms of 762 ± 5.8 emu · cm^{-3}, which was obtained experimentally from the continuous film deposited at the same time with the nanowires) were used in the dynamic simulation. The exchange length is defined as $l_{ex} = \sqrt{2A\mu_0/M_S^2}$. These parameters give the exchange length of 5.9 nm. The mask in the simulation was discretized in cells with a size of 9.4 nm×7.0 nm×10 nm and two-dimensional periodic boundary conditions were used. Simulation performed with a smaller cell size of 9.4 nm×7.0 nm×5 nm shows the same results. The total simulated volume was 1200 nm×900 nm×sample thickness (60 nm). For the quasistatic simulation, a damping coefficient of $\alpha = 1$ was chosen to obtain a rapid convergence. The FMR spectra were obtained by calculating the real part

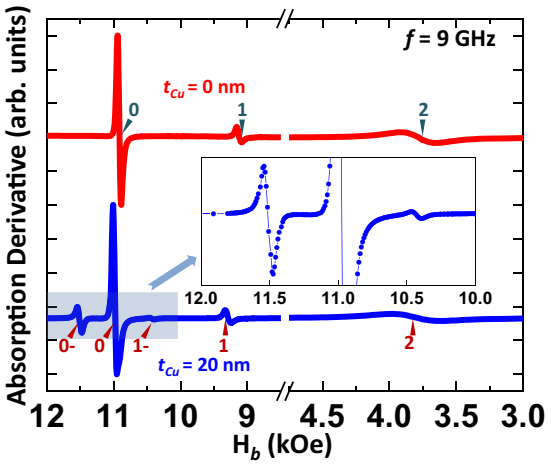

FIG. 2. Comparison of the experimental FMR spectra between $t_{Cu} = 0$ and 20 nm for $f = 9$ GHz. The inset shows a zoom-in of the FMR spectra in the field range from 12 kOe to 10 kOe.

of the dynamic susceptibility. In our LLG simulation, the ac excitation field was set at 10 Oe. The mode profiles were quantified by running another dynamic simulation with Chi pulse applied and analyzing the results using spatially and frequency-resolved fast Fourier transform (FFT) imaging.

III. RESULTS AND DISCUSSION

Shown in Fig. 2 is the comparison of typical FMR spectra taken at $f = 9$ GHz for $t_{Cu} = 0$ and 20 nm. For the single layer nanowires ($t_{Cu} = 0$ nm), three modes are observable with two resonance modes (modes 0, 1) detected in the saturation region and the other mode (mode 2) emerging in the low field region. Similar to what has been reported for structures of other geometries [33,40], the most intense mode appearing at the highest bias field ($H_b = 10.91$ kOe) is the fundamental mode with no nodal line ($n = 0$), while the other resonance mode observed at a lower bias field ($H_b = 9.33$ kOe) is the first order mode ($n = 1$) as a result of the finite width of the nanowires. As the higher order mode couples less efficiently with the rf field, it exhibits a much smaller intensity when compared with the fundamental mode. The broad resonance peak observed at $H_b = 3.79$ kOe originates from the nonuniform spin distribution [43], which has reorientated from out-of-plane to in-plane as the bias field is reduced. This also accounts for the large linewidth of the resonance peak. As the thickness of the spacer layer is increased from 0 to 20 nm, a more complex FMR spectrum is obtained. Besides modes 0, 1 in the saturation region and mode 2 for the unsaturated state, two additonal resonance modes are observed for $t_{Cu} = 20$ nm. Shown as the inset is a zoom-in of the FMR spectrum in the field range from 12 kOe to 10 kOe to better visualize the mode 0- and 1-. This is markedly different from what was observed for $t_{Cu} = 0$ nm. In particular, two additional resonance modes are present, with one located at $H_b = 11.52$ kOe and the other emerging at $H_b = 10.44$ kOe. Based on what was reported before for the trilayer nanowires magnetized in plane [44], mode 0- is attributed to be the optical mode with the magnetization in the upper and lower

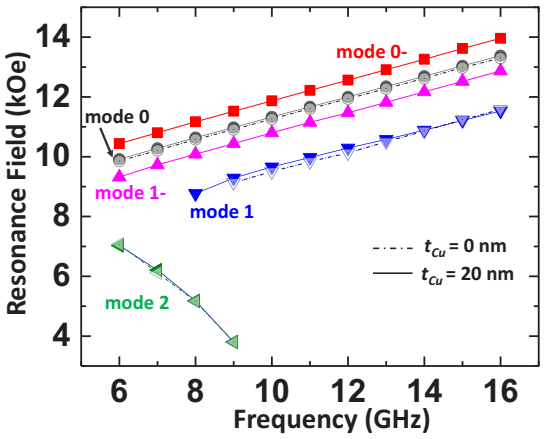

FIG. 3. Resonance fields of modes 0-, 0, 1-, 1, and 2 as a function of frequency ($f = 6 \sim 16$ GHz) for $t_{Cu} = 0$ and 20 nm.

$Ni_{80}Fe_{20}$ nanowires precessing out of phase, and this optical mode is more localized in the lower $Ni_{80}Fe_{20}$ nanowire arrays ($t = 10$ nm). As the out of phase precession is energetically more favorable due to the dipolar coupling arising from the surface magnetic charges at the lateral edges of the nanowires, the optical mode without nodal lines is expected to appear at a higher bias field than the fundamental acoustic mode (mode 0). Mode 1- will be discussed in detail later. What we may also notice is that as t_{Cu} is increased from 0 to 20 nm, mode 0 and 1 shift left while mode 2 shifts to a lower field position.

To further understand how the modes evolve with the excitation frequency, we have extracted the resonance fields as a function of frequency for both $t_{Cu} = 0$ and 20 nm. As presented in Fig. 3, three modes are observed for $t_{Cu} = 0$ nm. With an increase in the excitation frequency, the resonance fields for modes 0 and 1 increase monotonously. This could be explained by the dispersion equation [33,45,46],

$$\omega_k^2 = [\omega_H + \alpha\omega_M k^2][\omega_H + \alpha\omega_M k^2 + \omega_M f(kL)] \quad (1)$$

where $\omega_H = \gamma H_i$, $H_i = H_b - 4\pi M_S N_n(k)$, $\omega_M = \gamma 4\pi M_S$, $f(kL) = 1 - \frac{[1-\exp(-kL)]}{kL}$, k is the modulus of the in-plane wave vector, and $N_n(k)$ is the space dependent demagnetizing factor along z direction. As the excitation frequency (ω_k) is increased, ω_H increases correspondingly, thus resulting in a higher resonance field (H_b). Different from the dispersion relation for modes 0 and 1, mode 2 is a soft resonance mode showing a negative frequency evolution. As the excitation frequency is increased from 6 GHz to 9 GHz, the resonance field reduces from 7.06 kOe to 3.80 kOe. Similar behaviors were previously reported for other inhomogeneous equilibrium states, such as nanowires magnetized transversely [43,47], dots and rings in vortex states [48,49]. For $t_{Cu} = 20$ nm, a similar trend is observed. The resonance fields for mode 0-, 0, 1-, and 1 increase with a higher excitation frequency, while mode 2 varnishes gradually. Moreover, we also noticed that the resonance field of mode 0 for $t_{Cu} = 20$ nm is slightly higher than that for $t_{Cu} = 0$ nm ($\Delta H \sim 70$ Oe). This is because for $t_{Cu} = 20$ nm, the upper and lower $Ni_{80}Fe_{20}$ nanowires are exchange decoupled and act as individual layers. The acoustic fundamental mode, in such a situation, is formed on the base of the resonance in the upper layer ($t = 30$ nm),

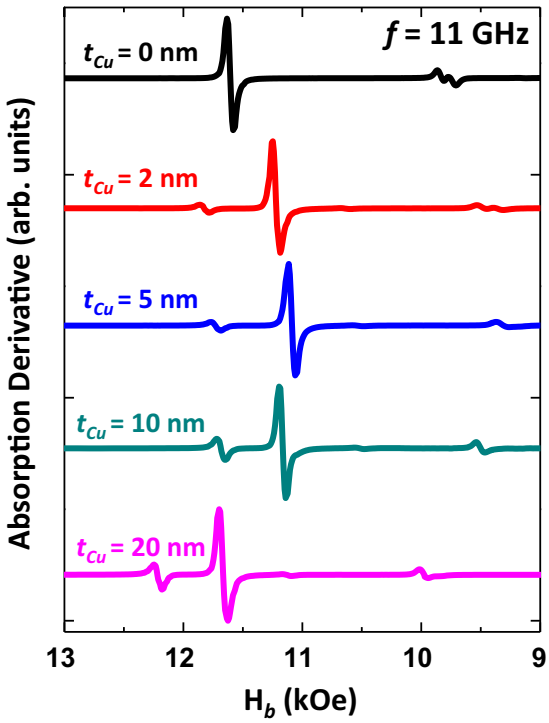

FIG. 4. Experimental FMR spectra for multilayer nanowire arrays taken at $f = 11$ GHz for $t_{Cu} = 0$, 2, 5, 10, 20 nm.

which has a larger effective demagnetizing factor along z direction [15] than that for 40 nm thick $Ni_{80}Fe_{20}$ nanowire arrays ($t_{Cu} = 0$ nm), thus leading to a higher resonance field.

Shown in Fig. 4 are the FMR absorption curves taken at $f = 11$ GHz for nanowires as a function of t_{Cu}. For the convenience of comparison, all the spectra were normalized to the intensity of the strongest mode. The fundamental mode and first order acoustic mode are observed for all the nanowire arrays. The optical mode (mode 0-) appears with the presence of 2 nm thick Cu spacer layer and becomes pronounced as t_{Cu} is increased. For all the trilayer structures, up to four resonance modes are observed in the saturation region. These modes show a similar trend with increasing Cu spacer thickness. Mode 1- is not visible due to the small intensity. For the fundamental acoustic mode (mode 0), as t_{Cu} is increased from 0 to 5 nm, the resonance field reduces monotonously from 11.61 kOe to 10.74 kOe. Mode 0 has a minimum value of the resonance field at $t_{Cu} = 5$ nm. As t_{Cu} is further increased from 5 to 20 nm, the resonance mode shifts upwards to a field value of 11.67 kOe. To better understand the effect of spacer thickness on the resonance field, we extracted the resonance fields of mode 0-, 0, and 1 as a function of t_{Cu}, as shown in Fig. 5(a). As aforementioned, the resonance fields for these modes drop in the beginning and reach the minimum at $t_{Cu} = 5$ nm. This decrease in the resonance fields suggests the decay of interlayer coupling. With an increasing Cu thickness, the upper and lower $Ni_{80}Fe_{20}$ nanowire arrays are less likely to be perfectly aligned along the z direction, resulting in more accumulation of the magnetic dipole charges at the lateral surface. Hence, the effective demagnetizing factor along the z direction becomes smaller, and thus the resonance field

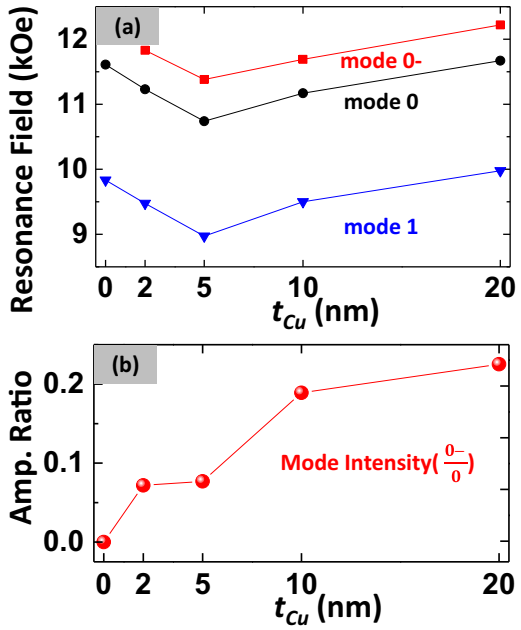

FIG. 5. (a) Resonance fields of modes 0-, 0, and 1 extracted as a function of Cu thickness ($t_{Cu} = 0 \sim 20$ nm). (b) Amplitude ratio between mode 0- and 0 as a function of Cu thickness ($t_{Cu} = 0 \sim 20$ nm).

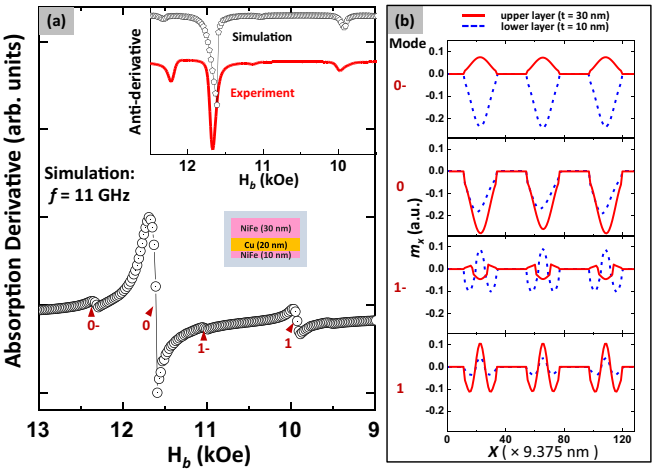

FIG. 6. (a) Simulated FMR spectra for $t_{Cu} = 20$ nm at $f = 11$ GHz. Shown as the inset is a comparison between the antiderivative of the experimental and simulated FMR spectra for $t_{Cu} = 20$ nm at $f = 11$ GHz. (b) Simulated distributions of dynamic magnetization for modes 0-, 0, 1-, and 1 in the lower (blue dash line) and upper (red solid line) nanowire arrays, respectively.

reduces. Despite the fact that the dipolar interaction is weaker with a thicker Cu layer, the reduced resonance fields indicate that the effect of the weakening interlayer exchange coupling is more significant when $t_{Cu} \leqslant 5$ nm. As the spacer layer further increases, the resonance fields increase. When the Cu thickness is larger than 5 nm, the upper and lower $Ni_{80}Fe_{20}$ nanowires are exchange decoupled. In this case, the interlayer exchange coupling is negligible, and only the dipolar interaction is dominant. With a thicker Cu layer, the dipolar interaction becomes weaker, and, therefore, the resonance fields become higher. Moreover, the intensity ratio of mode 0- over mode 0 was also extracted as a function of t_{Cu}, as shown in Fig. 5(b). With an increase in Cu thickness, the amplitude ratio increases monotonously from 0 ($t_{Cu} = 0$ nm) to 0.225 ($t_{Cu} = 20$ nm). The emergence of the optical mode for $t_{Cu} = 2$ nm evidences the separation of the acoustic and optical modes in the upper and lower nanowire arrays due to the symmetry breaking of the system [12]. However, this separation is not complete because of the existence of the interlayer exchange coupling. As the Cu thickness is increased from 2 nm to 10 nm, the amplitude ratio doubles (0.072 for $t_{Cu} = 2$ nm, 0.189 for $t_{Cu} = 10$ nm). This increase in the intensity ratio implies a further separation of the fundamental acoustic and optical modes resulting from the absence of the interlayer exchange coupling. With an increasing Cu thickness, the two $Ni_{80}Fe_{20}$ layers tend to act more like individual layers, and the acoustic (optical) mode gets more localized in the upper (lower) nanowires.

Shown in Fig. 6(a) is the simulated FMR spectrum for $t_{Cu} = 20$ nm at $f = 11$ GHz. In agreement with the experimental FMR spectrum shown in Fig. 4, four distinct modes are observed in the simulation result with the fundamental mode present at 11.61 kOe and the first order mode located at 9.93 kOe. Shown as the inset is a comparison of the antiderivative between the experimental and simulated FMR spectra. The simulation result is in quantitative agreement with the experimenal FMR absorption curve. Shown in Fig. 6(b) are the simulated distributions of the dynamic magnetization through the width of the upper (red solid line) and lower (blue dash line) nanowires for the four modes. These simulated distributions of magnetization show that the spin wave modes are all pinned at the lateral edges of the nanowires. As discussed before, mode 0 is the fundamental mode with no nodal line. The simulated modal distributions demonstrate the in phase precession of the upper and lower $Ni_{80}Fe_{20}$ nanowires (acoustic mode) with a larger precession amplitude in the upper $Ni_{80}Fe_{20}$ nanowires. Mode 0-, which is energetically more stable for the trilayer nanowire structures, appears at a higher bias field ($H_b = 12.31$ kOe) than the fundamental acoustic mode. As seen from the simulated magnetization distributions, the spin precession in the upper $Ni_{80}Fe_{20}$ nanowire array is suppressed while the lower $Ni_{80}Fe_{20}$ nanowire array has a larger precession amplitude. These simulation results have validated our previous discussion that the acoustic mode is more localized in the 30 nm thick $Ni_{80}Fe_{20}$ nanowires, while the optical mode is formed on the base of the resonance in the 10 nm thick $Ni_{80}Fe_{20}$ nanowires. Interestingly, mode 1- observed at $H_b = 11.01$ kOe is shown to be another optical mode, with the upper and lower nanowire arrays precessing out of phase. Similar to mode 0-, mode 1- is more localized in the lower nanowire arrays. As depicted by the simulated modal distributions, mode 1- is a higher order mode ($n = 1$), and for the upper nanowires array the resonance absorption is more locazlized in the center of the nanowire. In agreement with what was discussed before, mode 1 is the first order mode with the upper and lower nanowires precessing in phase. Similar to the fundamental mode, the upper nanowire arrays contribute more to the resonance absorption.

IV. CONCLUSION

We have probed the spin wave modes in asymmetric trilayer permalloy nanowire structures as a function of the Cu thickness using pFMR. We observed both the fundamental and first order modes in the saturation region for the 40 nm thick single layer $Ni_{80}Fe_{20}$ nanowires. However, for the trilayer structures more complex FMR spectra with two additional modes—the fundamental and first order optical modes—are observed. We found that the resonance fields of these resonance modes are markedly sensitive to the Cu thickness due to the competing effects of interlayer exchange coupling and magnetostatic dipolar coupling. As the thickness of the Cu layer is increased, the fundamental optical mode exhibits a larger intensity. Our experimental results were quantitatively validated using micromagnetic simulations.

ACKNOWLEDGMENTS

This work was supported by the National Research Foundation, Prime Minister's Office, Singapore under its Competitive Research Programme (CRP Award No. NRF-CRP 10-2012-03). A.O.A is a member of the Singapore Spintronics Consortium (SG-SPIN).

[1] J. Shibata, K. Shigeto, and Y. Otani, Phys. Rev. B **67**, 224404 (2003).
[2] R. Arias and D. L. Mills, Phys. Rev. B **67**, 094423 (2003).
[3] Z. Duan, I. N. Krivorotov, R. E. Arias, N. Reckers, S. Stienen, and J. Lindner, Phys. Rev. B **92**, 104424 (2015).
[4] C. Mathieu, J. Jorzick, A. Frank, S. O. Demokritov, A. N. Slavin, B. Hillebrands, B. Bartenlian, C. Chappert, D. Decanini, F. Rousseaux, and E. Cambril, Phys. Rev. Lett. **81**, 3968 (1998).
[5] F. G. Aliev, J. F. Sierra, A. A. Awad, G. N. Kakazei, D.-S. Han, S.-K. Kim, V. Metlushko, B. Ilic, and K. Y. Guslienko, Phys. Rev. B **79**, 174433 (2009).
[6] S. Choi, K.-S. Lee, K. Y. Guslienko, and S.-K. Kim, Phys. Rev. Lett. **98**, 087205 (2007).
[7] A. A. Nikitin, A. B. Ustinov, A. A. Semenov, A. V. Chumak, A. A. Serga, V. I. Vasyuchka, E. Lähderanta, B. A. Kalinikos, and B. Hillebrands, Appl. Phys. Lett. **106**, 102405 (2015).
[8] A. Haldar, D. Kumar, and A. O. Adeyeye, Nat. Nano. **11**, 437 (2016).
[9] Z. Duan, A. Smith, L. Yang, B. Youngblood, J. Lindner, V. E. Demidov, S. O. Demokritov, and I. N. Krivorotov, Nat. Commun. **5**, 5616 (2014).
[10] J. Ding, M. Kostylev, and A. O. Adeyeye, Phys. Rev. Lett. **107**, 047205 (2011).
[11] J. Ding, M. Kostylev, and A. O. Adeyeye, Appl. Phys. Lett. **100**, 073114 (2012).
[12] M. Kostylev, Z. Yang, I. S. Maksymov, J. Ding, S. Samarin, and A. O. Adeyeye, J. Appl. Phys. **119**, 103903 (2016).
[13] V. Vlaminck and M. Bailleul, Science **322**, 410 (2008).
[14] J. S. Kim, M. Stärk, M. Kläui, J. Yoon, C. Y. You, L. Lopez-Diaz, and E. Martinez, Phys. Rev. B **85**, 174428 (2012).
[15] J. Ding, M. Kostylev, and A. O. Adeyeye, Phys. Rev. B **84**, 054425 (2011).
[16] J. Topp, D. Heitmann, M. P. Kostylev, and D. Grundler, Phys. Rev. Lett. **104**, 207205 (2010).
[17] M. P. Kostylev, A. A. Stashkevich, and N. A. Sergeeva, Phys. Rev. B **69**, 064408 (2004).
[18] S. Tacchi, M. Madami, G. Gubbiotti, G. Carlotti, S. Goolaup, A. O. Adeyeye, N. Singh, and M. P. Kostylev, Phys. Rev. B **82**, 184408 (2010).
[19] M. Kostylev, P. Schrader, R. L. Stamps, G. Gubbiotti, G. Carlotti, A. O. Adeyeye, S. Goolaup, and N. Singh, Appl. Phys. Lett. **92**, 132504 (2008).
[20] G. Gubbiotti, S. Tacchi, G. Carlotti, P. Vavassori, N. Singh, S. Goolaup, A. O. Adeyeye, A. Stashkevich, and M. Kostylev, Phys. Rev. B **72**, 224413 (2005).
[21] M. P. Kostylev and A. A. Stashkevich, Phys. Rev. B **81**, 054418 (2010).
[22] Z. K. Wang, V. L. Zhang, H. S. Lim, S. C. Ng, M. H. Kuok, S. Jain, and A. O. Adeyeye, Appl. Phys. Lett. **94**, 083112 (2009).
[23] Z. K. Wang, V. L. Zhang, H. S. Lim, S. C. Ng, M. H. Kuok, S. Jain, and A. O. Adeyeye, ACS Nano **4**, 643 (2010).
[24] V. L. Zhang, H. S. Lim, C. S. Lin, Z. K. Wang, S. C. Ng, M. H. Kuok, S. Jain, A. O. Adeyeye, and M. G. Cottam, Appl. Phys. Lett. **99**, 143118 (2011).
[25] H. T. Nguyen and M. G. Cottam, AIP Conf. Proc. **1147**, 117 (2009).
[26] X. M. Liu, P. Lupo, M. G. Cottam, and A. O. Adeyeye, J. Appl. Phys. **118**, 113902 (2015).
[27] G. Gubbiotti, H. T. Nguyen, R. Hiramatsu, S. Tacchi, M. G. Cottam, and T. Ono, J. Magn. Magn. Mater. **384**, 45 (2015).
[28] G. Gubbiotti, S. Tacchi, H. T. Nguyen, M. Madami, G. Carlotti, K. Nakano, T. Ono, and M. G. Cottam, Phys. Rev. B **87**, 094406 (2013).
[29] B. Heinrich, Y. Tserkovnyak, G. Woltersdorf, A. Brataas, R. Urban, and G. E. W. Bauer, Phys. Rev. Lett. **90**, 187601 (2003).
[30] P. Grünberg, R. Schreiber, Y. Pang, M. B. Brodsky, and H. Sowers, Phys. Rev. Lett. **57**, 2442 (1986).
[31] S. Mizukami, Y. Ando, and T. Miyazaki, Phys. Rev. B **66**, 104413 (2002).
[32] R. Topkaya, M. Erkovan, A. Öztürk, O. Öztürk, B. Aktaş, and M. Özdemir, J. Appl. Phys. **108**, 023910 (2010).
[33] G. N. Kakazei, P. E. Wigen, K. Y. Guslienko, V. Novosad, A. N. Slavin, V. O. Golub, N. A. Lesnik, and Y. Otani, Appl. Phys. Lett. **85**, 443 (2004).
[34] D. Cimpoesu, J. Ding, L. Stoleriu, A. Adeyeye, A. Stancu, and L. Spinu, Appl. Phys. Lett. **102**, 232401 (2013).
[35] J. Ding, V. E. Demidov, M. G. Cottam, S. O. Demokritov, and A. O. Adeyeye, Appl. Phys. Lett. **104**, 143105 (2014).
[36] C. Du, R. Adur, H. Wang, A. J. Hauser, F. Yang, and P. C. Hammel, Phys. Rev. Lett. **110**, 147204 (2013).
[37] Y. Q. He and P. E. Wigen, J. Magn. Magn. Mater. **53**, 115 (1985).
[38] Y. Gong, Z. Cevher, M. Ebrahim, J. Lou, C. Pettiford, N. X. Sun, and Y. H. Ren, J. Appl. Phys. **106**, 063916 (2009).
[39] E. N. Ivanov and M. Kostylev, arXiv:1402.3459 (2014).

[40] X. Zhou, D. Kumar, I. S. Maksymov, M. Kostylev, and A. O. Adeyeye, Phys. Rev. B **92**, 054401 (2015).

[41] A. O. Adeyeye and N. Singh, J. Phys. D: Appl. Phys. **41**, 153001 (2008).

[42] M. R. Scheinfein, LLG Micromagnetics Simulator, software for micromagnetic simulations, http://llgmicro.home.mindspring.com (Date of access: 04.04.2014).

[43] J. Jorzick, S. O. Demokritov, B. Hillebrands, M. Bailleul, C. Fermon, K. Y. Guslienko, A. N. Slavin, D. V. Berkov, and N. L. Gorn, Phys. Rev. Lett. **88**, 047204 (2002).

[44] G. Gubbiotti, M. Kostyleva, N. Sergeevaa, M. Conti, G. Carlotti, T. Ono, A. N. Slavin, and A. Stashkevich, Phys. Rev. B **70**, 224422 (2004).

[45] B. A. Kalinikos and A. N. Slavin, J. Phys. C: Solid State Phys. **19**, 7013 (1986).

[46] B. A. Kalinikos, M. P. Kostylev, N. V. Kozhus, and A. N. Slavin, J. Phys.: Condens. Matter **2**, 9861 (1990).

[47] C. Bayer, J. P. Park, H. Wang, M. Yan, C. E. Campbell, and P. A. Crowell, Phys. Rev. B **69**, 134401 (2004).

[48] G. Gubbiotti, M. Madami, S. Tacchi, G. Carlotti, H. Tanigawa, T. Ono, L. Giovannini, F. Montoncello, and F. Nizzoli, Phys. Rev. Lett. **97**, 247203 (2006).

[49] V. Castel, J. BenYoussef, F. Boust, R. Weil, B. Pigeau, G. de Loubens, V. V. Naletov, O. Klein, and N. Vukadinovic, Phys. Rev. B **85**, 184419 (2012).